ENHANCING METAL ION SCAVENGER DELIVERY USING POROUS MATERIALS

by

Youanna Ibrahim

Submitted in partial fulfillment of the

requirements for Departmental Honors in

the Department of Chemistry and Biochemistry

Texas Christian University

Fort Worth, Texas

May 2, 2022

ENHANCING METAL ION SCAVENGER DELIVERY

USING POROUS MATERIALS

Project Approved:

Supervising Professor: Jeffery Coffer, Ph. D.

Department of Chemistry and Biochemistry

Kayla Green, Ph. D.

Department of Chemistry and Biochemistry

Giridhar Akkaraju, Ph. D.

Department of Biology

ABSTRACT

It is estimated that 50 million individuals worldwide live with Alzheimer's disease (AD), a neurodegenerative progressive disorder that, along with other chronic dementias, cost the United States $355 billion in 2021. Previous research links AD with amyloid beta (Aβ) aggregation in the brain. Possible therapeutic drugs, including antioxidants and metal chelating agents, need efficient delivery systems that can cross the blood-brain barrier and release drugs appropriately. Recent discoveries in nanoscale materials as targeted drug delivery and controlled release agents have shown that such materials can release therapeutic drugs in a slow manner and increase efficacy. Chief among these carriers are porous materials with high surface areas because of their tunable pore structure, surface chemistry and drug loading capacity. This project focuses on using porous silicon derivatives as a carrier because, in addition to the above properties, it is a known biocompatible material.

This research deals with developing efficient protocols for loading mesoporous silica ($pSiO_2$) with selected metal ion binding agents through systematic manipulation of external variables in order to achieve the highest percentage of loading. Once this has been determined, release and complexation studies are conducted. Known spectrophotometric methods are used to monitor diffusion over time and evaluate the profile of the sustained release. Different derivatives of macrocycles are loaded and released to determine the effects of structural characteristics. The macrocyclic molecule pyclen is the first tested candidate, followed by its dimer form, and finally a halogen substituted derivative. Stoichiometric complexation ratios with copper ions are then measured. Developing a slow and steady rate at which drugs capable of inhibiting neurotoxic Aβ aggregates in the brain can be released should be more effective and lead to more promising solutions for AD.

Acknowledgements

The completion of this work would not have been possible without the help and contribution of many members in the TCU Chemistry and Biochemistry Department.

It is my deepest honor to express my gratitude to my mentor, Dr. Jeffery Coffer, who has made every step of this process enjoyable and enriching. His guidance has helped shape this work and his support has been the best encouragement along the way. It has been a pleasure to be a part of his lab and I owe it to his undying excitement. I am deeply grateful for his wisdom and his encouraging chant, "Go, Youanna, go!" has been the push I needed to overcome many obstacles.

I would also like to thank my lab mates, Will, Nguyen, Leo, Maegyn, and Alexa who have supported me constantly, made our lab so enjoyable, and for willingly offering help and guidance any time it was needed. I am extremely grateful for Dr. Kayla Green and Kristof as well for sharing their knowledge and resources with me over the past years and helping me shape this work.

Finally, I would like to give special thanks to my family who has never stopped supporting and encouraging me. My parents and my sister have constantly pushed me to my best, rejoiced with me in the highs, and endured the lows with me. Their love has been the biggest gift and I am so blessed to call them mine.

Table of Contents

List of Figures

1 Introduction

In the United States alone, 6.5 million age 65 and older live with Alzheimer's Disease (AD), which is listed as the fifth-leading cause of death in 2021 for that segment of the population[1]. Official death certificates recorded 121,499 AD deaths in 2019. Since 2000, deaths caused by stroke, heart disease, and HIV decreased; deaths caused by AD, however, have increased by more than 145%. This also led to 16 billion hours of care to people with Alzheimer's or other dementias in 2021[1]. The need for new drugs for treating AD is thus of great and increasing significance.

As literature indicates, among the different theories for the causes and progression of AD, the majority point to an association between amyloid ß (Aß) protein aggregation in the brain with AD pathology[2]. The normal Aß protein, void of any misfolding, plays an essential role in neural growth and repair including protecting the body from infections, repairing leaks in the blood-brain barrier, promoting recovery from injury, and regulating synaptic function[3]. The aggregated neurotoxic Aß on the other hand can permeate cellular membranes and disturb cellular processes[4]. Oligomers of amyloid ß (AßO) play a major role in AD seeding[5]. AßO are highly toxic peptide assemblies with an ordered region and a shorter disordered region. The ordered region controls attachment and cellular entry and presents the disordered part for a specific cellular interaction wherein the toxicity lies[6].

The brain is highly vulnerable to oxidative damage resulting from unregulated redox-active metals such as copper (Cu) and iron (Fe). Metal dyshomeostasis and increased oxidative stress are common in AD patients[7]. Cu modulates neurotransmission in the brain, so its homeostasis is carefully regulated[8]. It affects the synapses by modulating the permeability of neurons and by complexing with different neurotransmitters[9]. Cu directly interacts with amyloid precursor proteins (APP) through their extracellular domains. APP regulates neural Cu homeostasis. Cu also

alters the activity of glycogen synthase kinase, an enzyme that regulates APP processing, linking Cu to APP biology through multiple mechanisms[10]. Aß is a Cu-binding peptide that disrupts the Cu-dependent interaction between cellular prion protein (PrP^C) and *N*-methyl-$_D$-aspartate receptor (NMDAR), inducing overactivation of NMDAR and neurotoxicity by competing with PrP^C for Cu[11]. The Cu-Aß complex in the neural synapse during NMDA-receptor-mediated neurotransmission provides a microenvironment that further induces the abnormal interaction of Aß with Cu under conditions of copper dysregulation prevalent in AD. This results in the formation of neurotoxic soluble AßO that continue aggregating to form amyloid plaques, a main pathological mark of AD[12]. These findings promote metal chelation therapy as a promising treatment method for AD.

An important aspect to consider when addressing AD drugs is the blood-brain barrier (BBB) which is composed of microvascular tight junctions and glial cell sheathing that selectively control drug permeation into the central nervous system (CNS)[13]. The BBB serves to protect the brain from toxic side effects. However, for therapeutic drugs to efficiently accomplish their purpose they must be able cross the BBB in therapeutic concentrations. Their ability to do so depends on the physiochemical properties of the drug molecules[14].

Pharmacologically active agents that manage and treat disease are not inherently effective, as they heavily rely on the manner of their administration and delivery. Drug pharmacokinetics, absorption, distribution, metabolism, duration of therapeutic effect, excretion, and toxicity are all affected by drug delivery. New therapeutic agents need improved chemistries and materials to deliver them to the target site in the body, at a therapeutic concentration, and for the required period of time[15]. Nanoparticles have emerged as promising delivery agents, especially to the brain because of their size[16].

Nanotechnology is the engineering and manufacturing of materials at the atomic and molecular scale. It refers to structures roughly in the 1−100 nm size range in at least one dimension but commonly refers to structures that are up to several hundred nanometers in size as well that are developed by top-down or bottom-up engineering of individual components[17]. Some of the parameters that are important for the successful development and manufacturing of targeted drug delivery vehicles include the use of biocompatible materials, the ability to optimize cell targeting and uptake, and developing scalable unit operations to manufacture large quantities of targeted drug delivery systems needed for clinical translation[18]. The bio-physicochemical properties of the vehicle, such as size, charge, surface hydrophilicity, and the nature and density of the ligands on their surface, can all impact the circulating half-life of the particles as well as their biodistribution[19]. **Figure 1** shows a depiction of nanoparticle uptake across vessel walls.

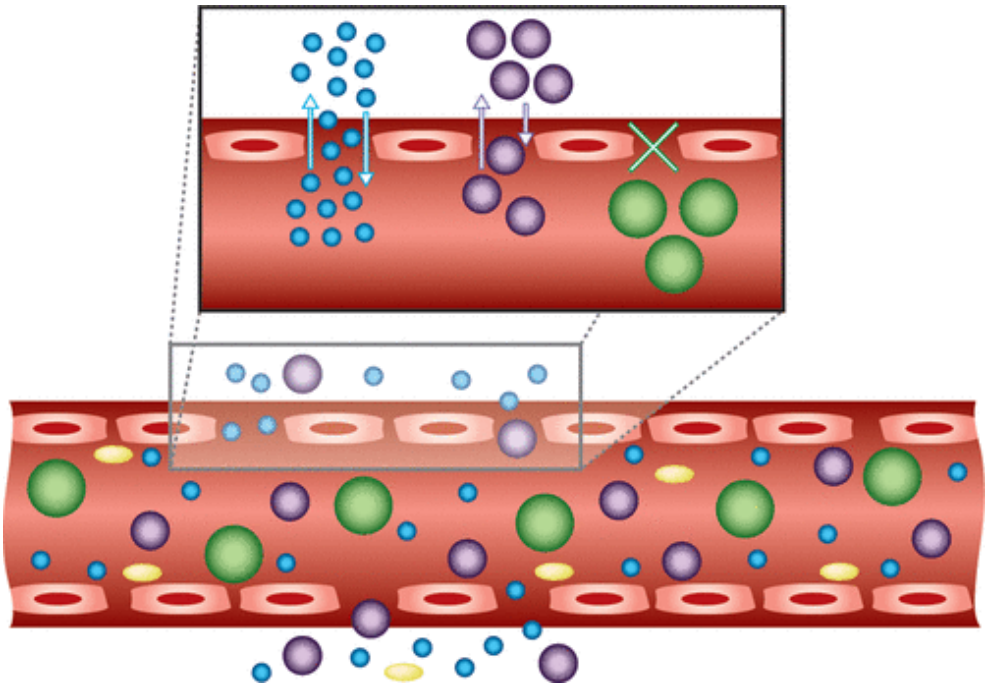

Figure 1. Nanoparticle efficacy as delivery vehicles highly depends on size and shape. Smaller vehicles are more easily diffused across the vessel walls than larger vehicles.[17]

Recent pharmaceutical research has focused on controlled drug delivery having an advantage over conventional methods. Controlled delivery has the potential for maximizing efficacy while minimizing dose frequency and toxicity[20]. **Figure 2** demonstrates the difference between a conventional drug release profile and a controlled release profile[21]. The conventional profile is observed in most medicinal drugs. After the first dose, a high burst effect is seen that leads to drug concentrations above the ideal therapeutic concentration range. This high concentration often leads to detrimental side effects. Furthermore, the release decreases relatively quickly over time until it is too small of a concentration to be effective and another dose would be needed yielding another burst effect. On the other hand, a controlled release profile, also referred to as a sustained release, minimizes the burst effect by slowing down the initial release and continuing it over a prolonged time period. Side effects are thus minimized and the drug concentration is kept within the ideal therapeutic range requiring less doses.

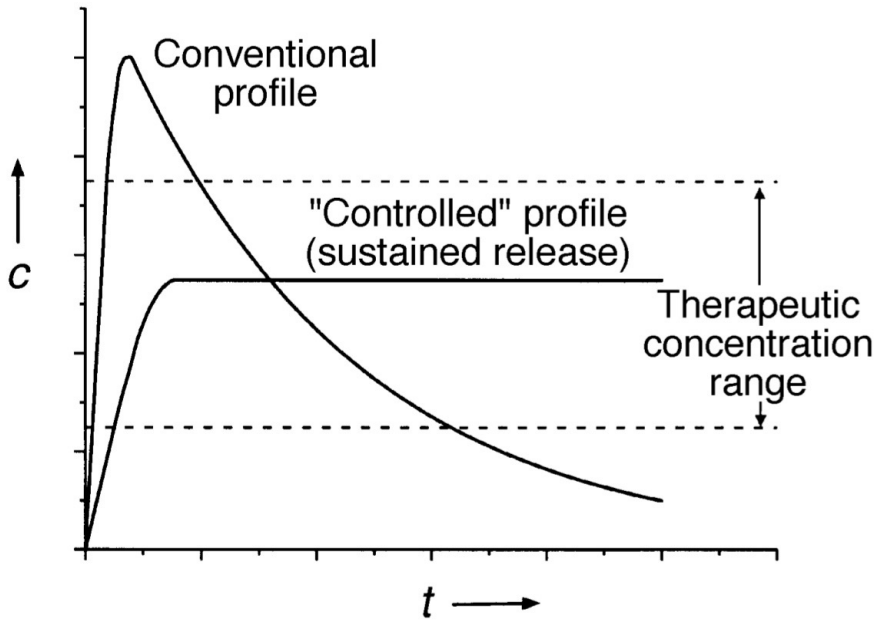

Figure 2. Comparison between the conventional and controlled release profile. The conventional profile demonstrates a burst effect while the controlled profile shows a sustained release. Concentration is referred to as *c* and time is referred to as *t*.[21]

Many drug delivery systems utilize a porous matrix which provides a large volume reservoir for the drugs[22]. The large surface area of porous materials provides a wide range of porosities and diverse surface chemistry that allows drug incorporation through various approaches. Different pore sizes can be used to adjust the loading of the molecules of interest. Nanostructured porous silicon (pSi) and its derivatives, such as mesoporous silica ($pSiO_2$), are versatile candidates for such systems because of their nontoxicity, biodegradability, and high tunability[23]. **Figure 3** shows the three approaches used in tuning pSi[24]. Some of the areas where pSi has proven useful include drug delivery, tissue engineering, and biosensing devices[23]. More applications for pSi and $pSiO_2$ are shown in **Figure 4**[25]. Furthermore, high surface area mesoporous silicon can be readily achieved through an ecofriendly synthesis route using silicon-accumulator plants as the starting materials. For example, the powder of silicon accumulator plant, bamboo Tabasheer, was used to fabricate pSi drug carriers by magnesiothermic reduction of plant-derived silica[26].

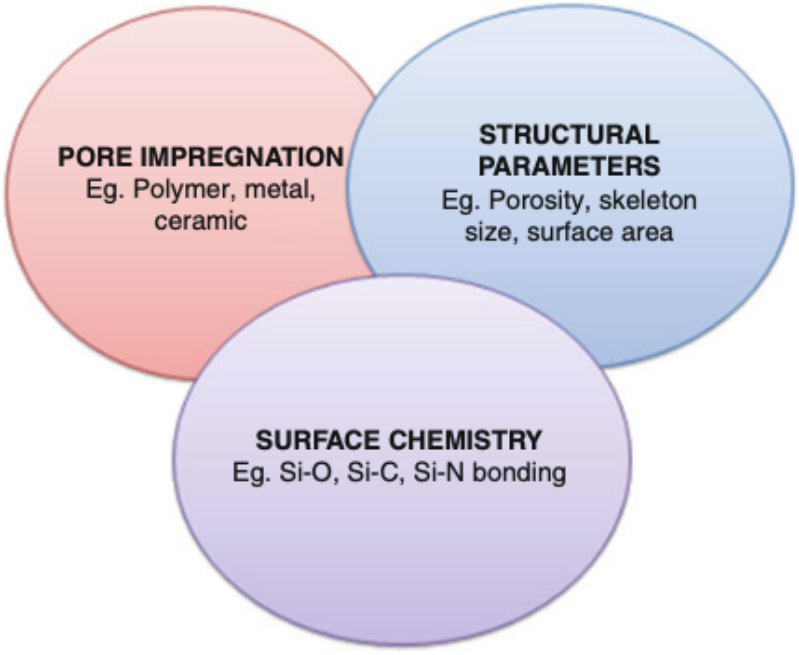

Figure 3. The three approaches to tuning properties of porous silicon.[24]

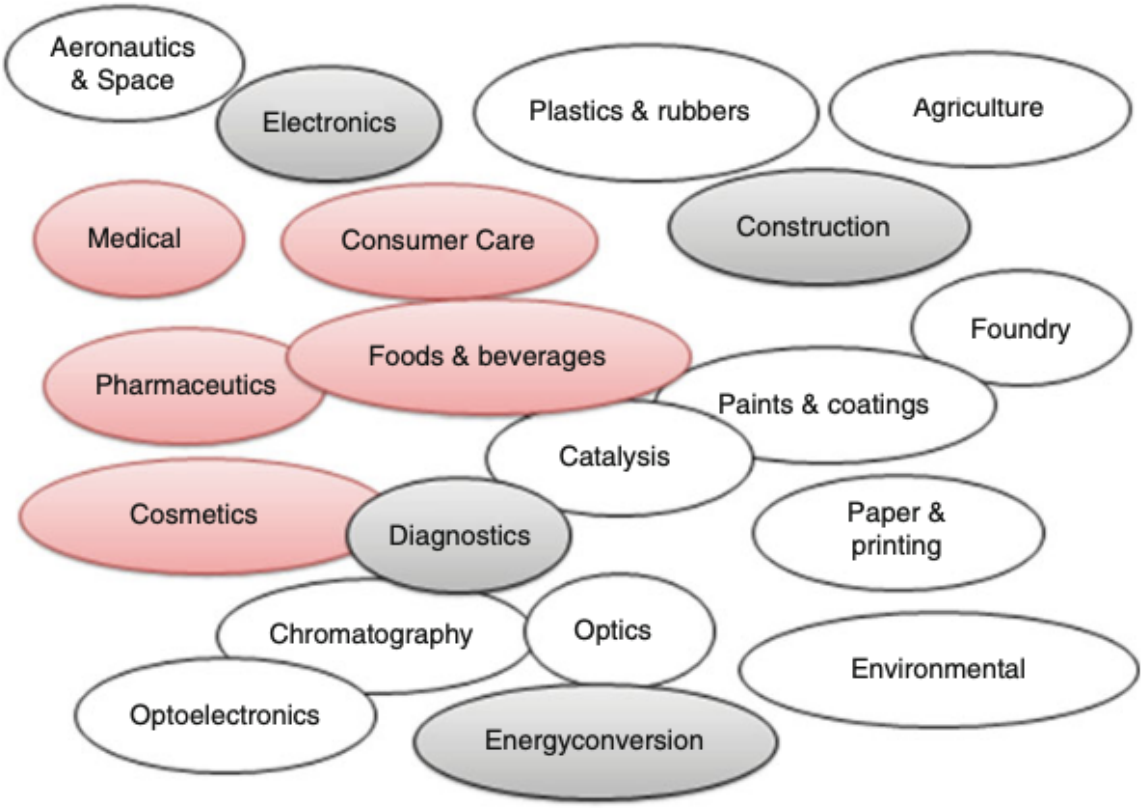

Figure 4. Application domains of silica, porous silica, silicon, and potentially porous silicon, arranged by typical product values. High-value sectors are to the left; low-value sectors to the right. Sectors with well-defined and regulated grades of material (silica in most cases) are in light red circles. Sectors which dominate industrial silica supply are in white circles; those that dominate industrial silicon supply are in light gray.[25]

The drug delivery system of porous nanoscale particles has been discussed with an explanation of its benefits. The drugs used in this system are addressed next. Oxidative stress, dyshomeostasis of metal ions, and protein aggregation are consistent components described in the development of many neurodegenerative diseases such as AD[27]. Imbalance between the reactive oxygen species (ROS) and the availability or activity of antioxidants leads to damage in the proteins, lipids, and DNA of the brain. Additionally, redox-active transition-metal ions are vital components of the brain for detoxification of free radicals, electron and oxygen transport processes, neurotransmitter biosynthesis, and neuronal signaling. Disruption in these systems

yields dysregulation of the redox-active metals, like Cu and Fe, promoting Aß aggregation. Disproportionately high levels of metal ions have been observed in the hallmark Aβ plaques. The drugs used in this work are new, potent small molecules that target oxidative stress and metal-ion misregulation[27]. **Figure 5** shows the molecules used as therapeutic agents. The four nitrogen atoms serve as the metal binding site, the pyridine ring serves as the antioxidant agent, and the substituents, when present, act as radical scavengers. Applications of these molecules as potential therapeutics for neurodegenerative diseases derived from oxidative stress have already been reported[27].

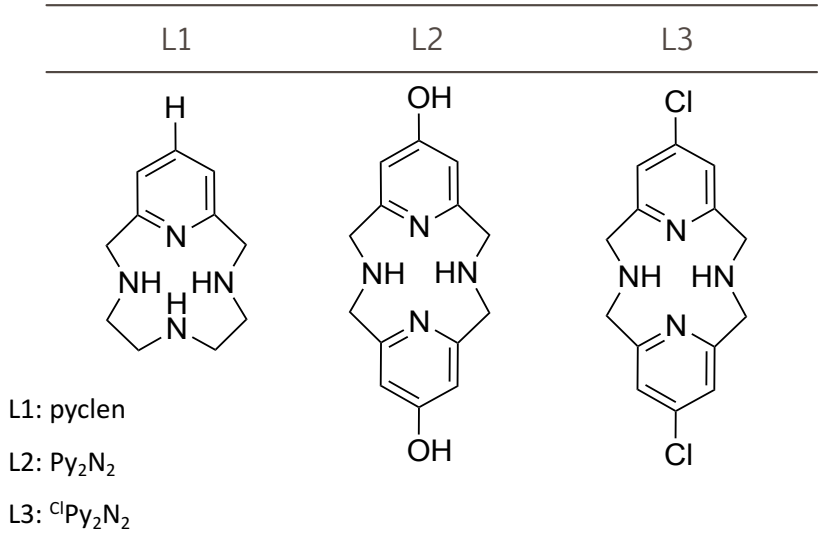

Figure 5. The structure of L1, L2, and L3 chelating agents.

Compound L1, also referred to as pyclen, was the first macrocycle to be tested. Factors such as the cavity size, denticity, flexibility, and the presence of substituents are all important structural elements deeply influencing the geometry of the metal coordination sphere and corresponding redox activity of the metal center[28]. As a result, macrocycles with different structural characteristics were tested next. Since the goal is to develop a sustained release delivery system, macrocycles that can be hypothesized to be better suited for the delivery system used were

the ones chosen to be studied. Bigger size was first hypothesized to be a better candidate for a drug to be carried by a nanoscale porous delivery system since the larger size might lead the macrocycles to remain stuck within the pores longer. This led to L2, the dimer OH-substituted derivative of pyclen commonly referred to as Py_2N_2, to be considered. The substituent group was hypothesized next to affect the rate of release leading to the testing of L3, the dimer Cl-substituted derivative of pyclen commonly referred to as $^{Cl}Py_2N_2$, to compare the difference between the hydrogen bonding of L2 and the negative charge of L3[29].

A silica-macrocycle drug delivery system has been reported by Wang et al of Nanjing University, Nanjing, P. R. China[30]. Their system used nanoscale nonporous silica particle as the carrier and covalently attached a cyclen molecule to the silica particles as the metal-chelating agent as shown in **Figure 6**. They report success in crossing the BBB because of the nanoscale size of their silica particles.

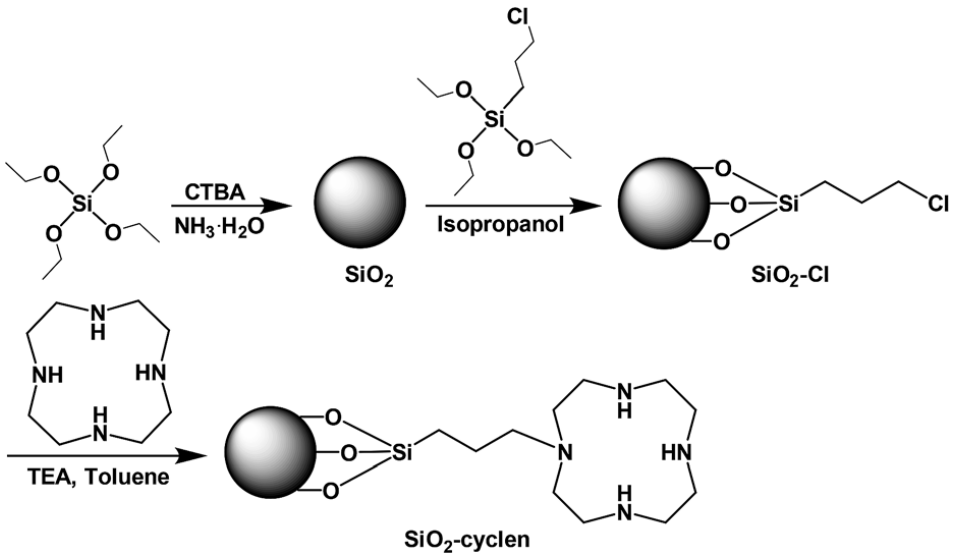

Figure 6. A schematic showing the silica-cyclen covalently bound composite used as a drug delivery system by Wang et al of Nanjing University. [30]

One issue that could arise with the SiO_2-cyclen structure is the exposed manner by which the chelating agent is held *in vivo*. The macrocycle could bind to other targets in the body before

reaching its target destination. As a result, the idea behind the SiO_2-cyclen composite was modified to ideally achieve a more efficient drug delivery system. In the work discussed here, mesoporous silica ($pSiO_2$) with particle size of 1 μm diameter and 2 nm pores, shown in the SEM image seen in **Figure 7**, is used instead of the nonporous SiO_2 to load the chelating agents inside the pores instead of the external covalent bonding. Furthermore, the chelating agents used in this work, L1, L2, and L3, have higher oxidative capabilities than cyclen since they contain pyridine rings.

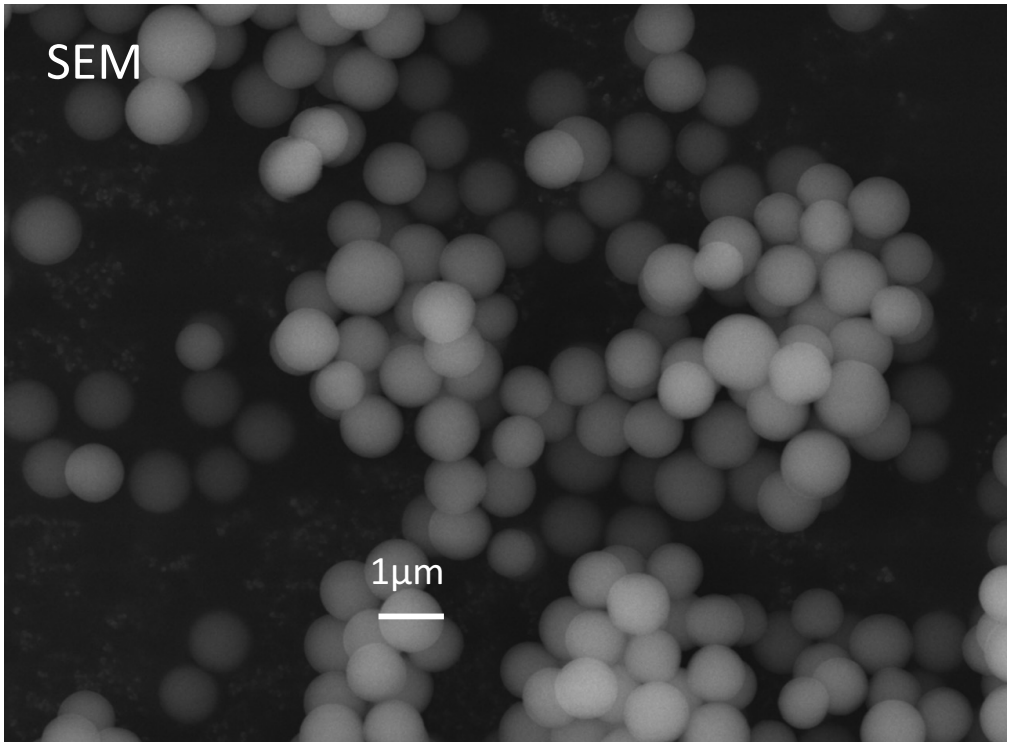

Figure 7. An SEM image of $pSiO_2$ particles, 1 μm in diameter and 2 nm pores. Image obtained from Will Burnett, TCU Chemistry and Biochemistry Department.

To measure this work, an efficient loading procedure is first developed followed by release studies to assess the kinetic profile of the $pSiO_2$ drug delivery system and the effects of the interactions between the $pSiO_2$ particles and the macrocycles based on their structural characteristics.

2 Experimental

2.1 Instrumentation.

The following instruments were used in this research:

- Thermo Scientific mySPIN 12 Centrifuge
- UV-Vis Spectrophotometer – Agilent Model: Cary 60
- VWR Incubating Orbital Shaker
- Buchi Rotary Evaporator

2.2 Calibration Curves

Calibration curves for the macrocycles in dimethyl sulfoxide (DMSO), hydroxyethyl piperazineethanesulfonic acid (HEPES), and HEPES in the presence of a 4 mM Cu (II) concentration were obtained. DMSO is used for measuring encapsulation efficiency, HEPES, shown in **Figure 8**, is the physiological buffer used to mimic body environment in the release studies, and HEPES with the presence of Cu (II) is used to mimic the presence of metal ions in the brain. A 4 mM Cu (II) concentration is used in order to provide an excess of Cu (as predicted to be the case starting with a 2:1 molar ratio of Cu: chelating agent at the highest concentration).

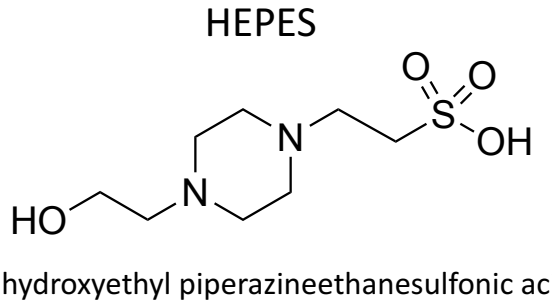

Figure 8. The structure of HEPES, the physiological buffer.

2.3 Making the Base Form of the Chelating Agents

The chelating agents (as HCl salts) are obtained from the Research Group of Professor Kayla Green of the TCU Department of Chemistry and Biochemistry. The basic, and less hydrophilic form, is preferred to achieve a slower release. To transform the above acid form to the free base, a concentrated NaOH solution is added to the macrocycle to raise the pH above 12. A rotary evaporator is used to evaporate the water, followed by the addition of ethanol to remove any remaining salts.

2.4 Incipient loading of Pyclen Derivatives into Porous Silica

This procedure is performed at 37 °C to mimic body temperature. **Figure 9** shows a schematic of the procedure. The $pSiO_2$ with 1µm diameter and 4 nm pores obtained from Sigma Aldrich is placed on a hotplate and the concentrated chelating agent solution, around 200 mM (dissolved in ethanol) is added in small 100 µL increments. The amount of chelating agent added is determined by targeting a 20% loading, a percentage chosen for its prevalence in medicinal drugs. The $pSiO_2$ is left on the plate until the solution evaporates and this is repeated until the solution containing the macrocycle has all been added. Pyclen and its derivatives are consequently absorbed into the pores of the $pSiO_2$.

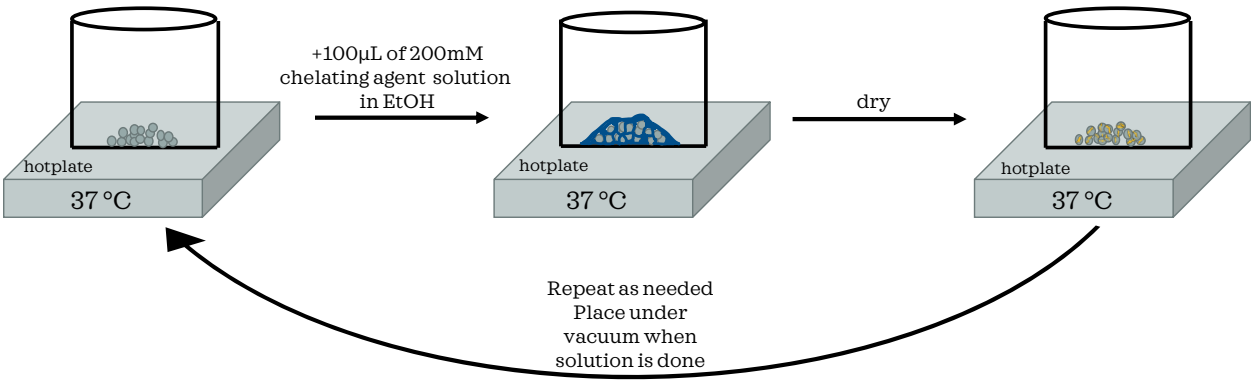

Figure 9. A visual representation of the incipient loading of pyclen derivatives into $pSiO_2$.

2.5 Release into HEPES Buffer and HEPES + Cu (II)

About 8 mg of the loaded $pSiO_2$ is placed in a centrifuge tube and exactly 1 mL of HEPES buffer or HEPES + Cu (II) is added. The centrifuge tube is incubated at 37 °C for 5 minutes and then centrifuged for 2 minutes as shown in **Figure 10**. The UV/Visible absorption spectrum of the supernatant is then measured using a spectrophotometer. The supernatant is then removed and a fresh 1 mL amount of HEPES buffer or HEPES + Cu (II) is added to mimic the body's constantly renewed fluid supply. The procedure is repeated with different incubation times and then release of macrocycles from silica is calculated cumulatively. Release with or without the presence of copper ions is performed in 3 trials each.

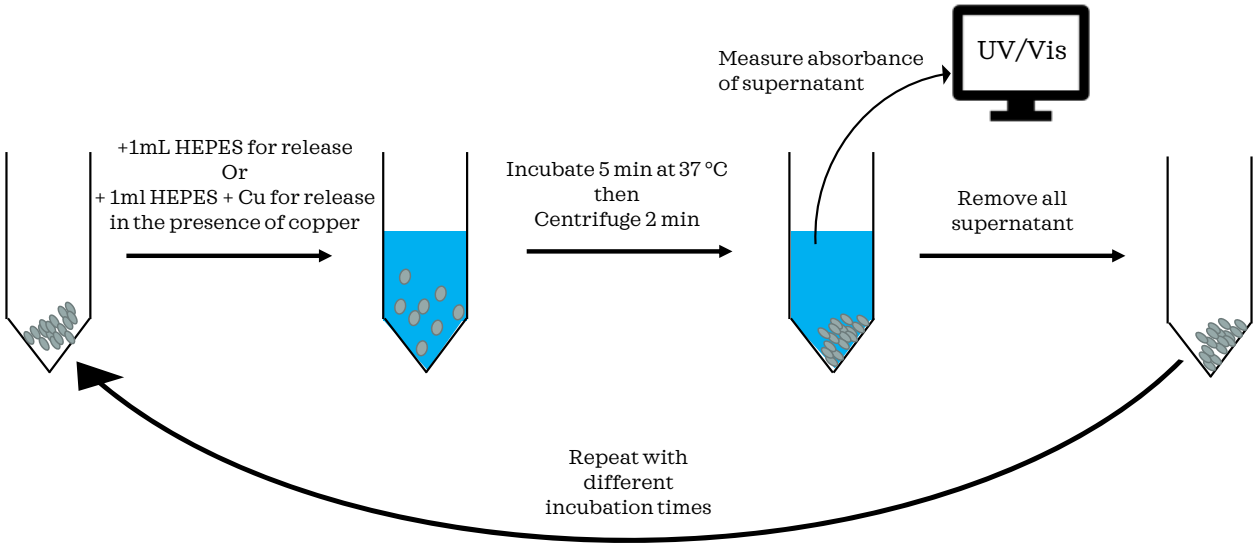

Figure 10. A visual representation of the release procedure of pyclen and its derivatives from $pSiO_2$.

This procedure is also used for measuring encapsulation efficiency. Encapsulation efficiency is a method used to measure the percent loading by mass of the macrocycles in the silica. It is needed to be able to measure release percent over time relative to the amount of macrocycle present in the silica sample used. The only difference in the procedure includes using 1 mL of

DMSO instead of the HEPES. DMSO is a strong solvent that effectively dissolves a given macrocycle and removes it from the porous carrier ($pSiO_2$).

3 Results and Discussion

3.1 Pyclen (L1) Loading and Release

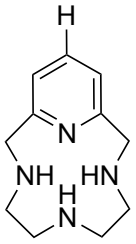

Figure 11. The structure of pyclen (L1)

Figure 11 shows L1 and **Figure 12** shows the calibration curves in each solvent of which the slope equation is used to calculate the concentration of the release procedure samples.

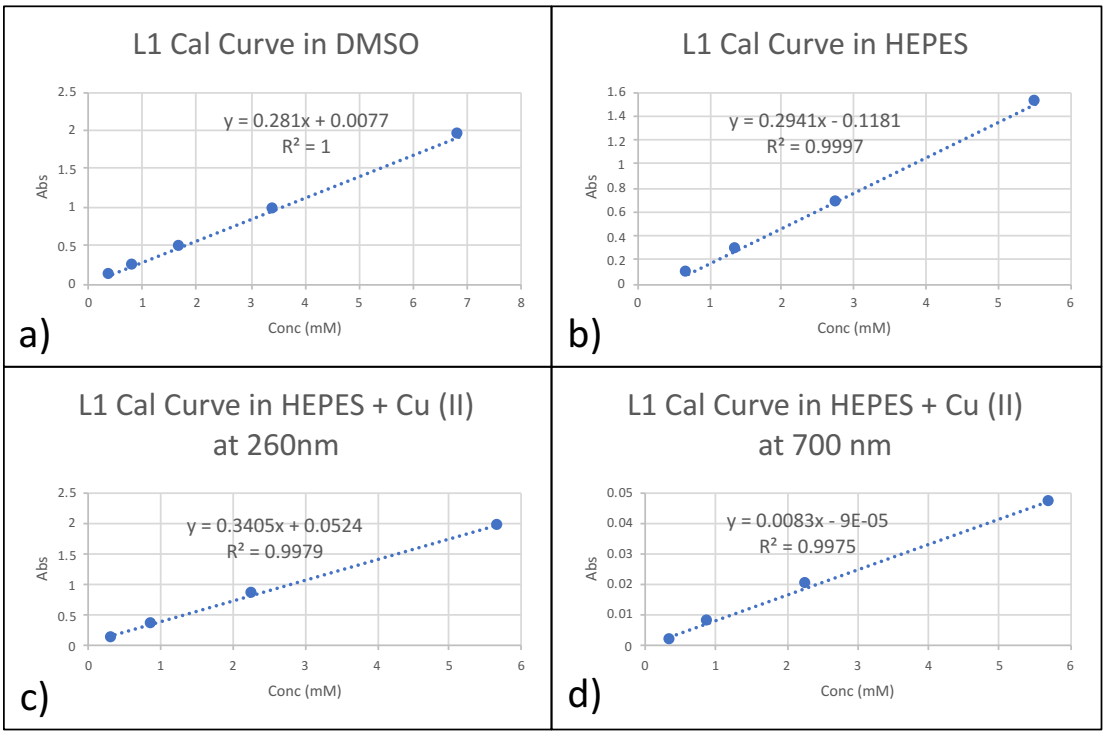

Figure 12. The L1 calibration curves in a) DMSO, b) HEPES, c) HEPES + Cu (II) at 260 nm, d) HEPES + Cu (II) at 700 nm. Absorbance is measured on the y-axis and concentration in mM is measured on the x-axis. The absorbance coefficients obtained are a) 0.281, b) 0.294, c) 0.341, d) 0.0083.

The coefficient in DMSO, **Figure 12a**, is needed for encapsulation efficiency determination. The coefficient in HEPES, **Figure 12b**, is used for the release studies. The reason release is repeated in the presence of Cu (II) is to determine whether the presence of Cu (II), which is the case in the brain, alters the rate of release. If the copper ions play a role in pulling the chelating agents out of the pores faster, either because of binding and changing the conformation of the macrocycles or because of Le Chatelier's principle, the release profile might be affected. This is why the absorption coefficient in HEPES + Cu (II) at 260 nm, **Figure 12c**, is needed. The 260 nm peak is associated with the π-π* transition of the pyridine rings of the macrocycles. Another advantage for performing release with copper is to measure the complexation rates. However, the absorption coefficient at 700 nm, **Figure 12d**, is too small to yield reliable data. The noise from the UV/Vis Spectrophotometer interferes with the absorption spectra at 700 nm overriding the d-d transition of the Cu-metal peak. The π-π* transition is inherently more intense than the d-d transition, as a result, only the 260 nm peak is used to quantify release.

The representative spectra shown in **Figure 13** demonstrate the difference in intensities of the π-π* transition vs. the d-d transition. The Cu-pyclen complex peak is only used in this case to confirm the complexation between the macrocycle and the Cu ions. No further data was collected for this wavelength range with L2 and L3. **Figure 13** shows the spectra collected during the release procedure at the different cumulative time marks. The peak absorbance value is used with the absorption coefficient to determine the concentration of the released therapeutic agent.

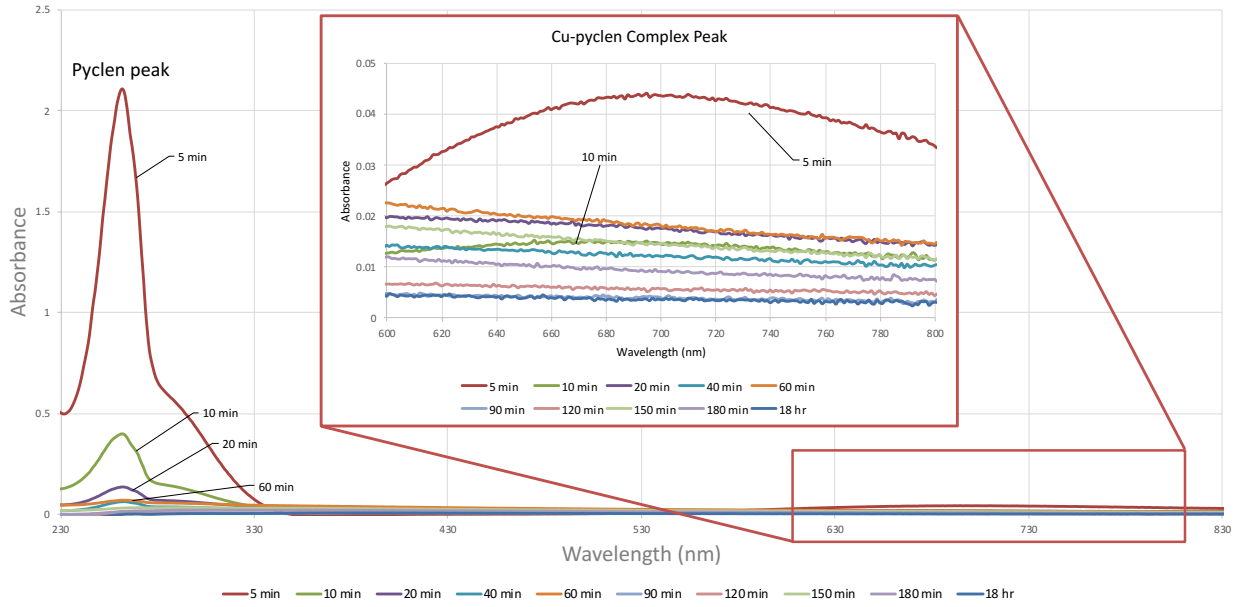

Figure 13. Representative spectra of pyclen release in the presence of Cu (II) showing both the pyclen and Cu-pyclen complex peaks.

Encapsulation efficiency for L1 was determined to be 17% as shown in **Figure 14**. This value was used to calculate the percent release in each of the release trials for L1.

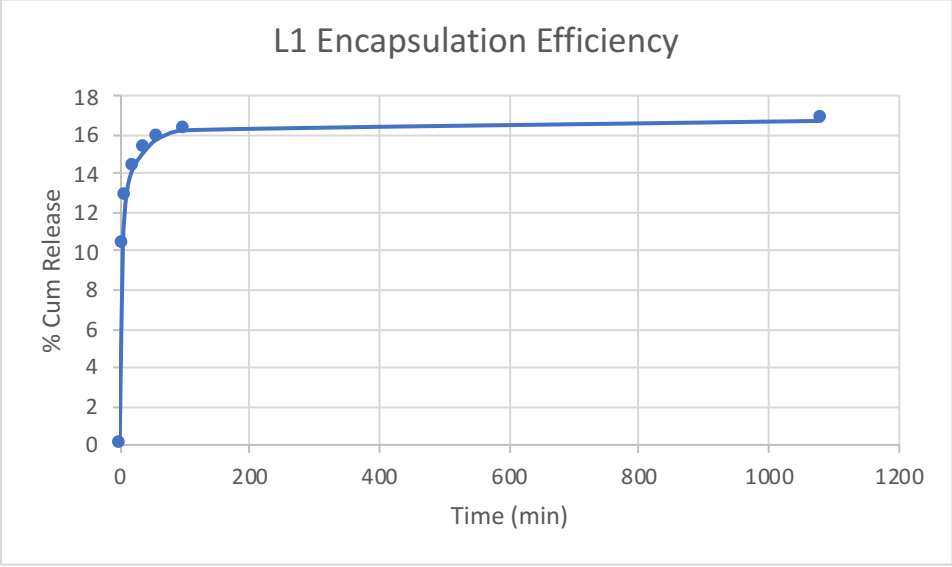

Figure 14. L1 encapsulation efficiency of 17% measured in DMSO.

The release profile of L1 from $pSiO_2$ in HEPES buffer is shown in **Figure 15**. The drug is released quickly with 50% of the L1 compound released within the first 10 minutes.

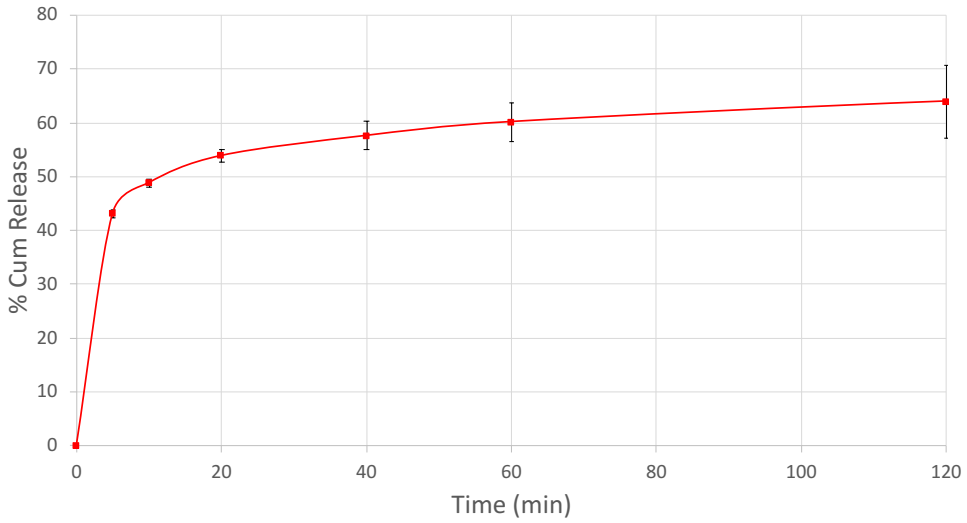

Figure 15. Cumulative release of L1 from $pSiO_2$ in HEPES buffer

When the release is done in the presence of Cu (II), the same burst effect is observed as seen in **Figure 16** with 70% of the loaded macrocycles released in the first 10 minutes. However, it is also observed that more of what is loaded is actually released in the presence of Cu (II), indicating the Cu (II) helps pull more macrocycles out of the silica.

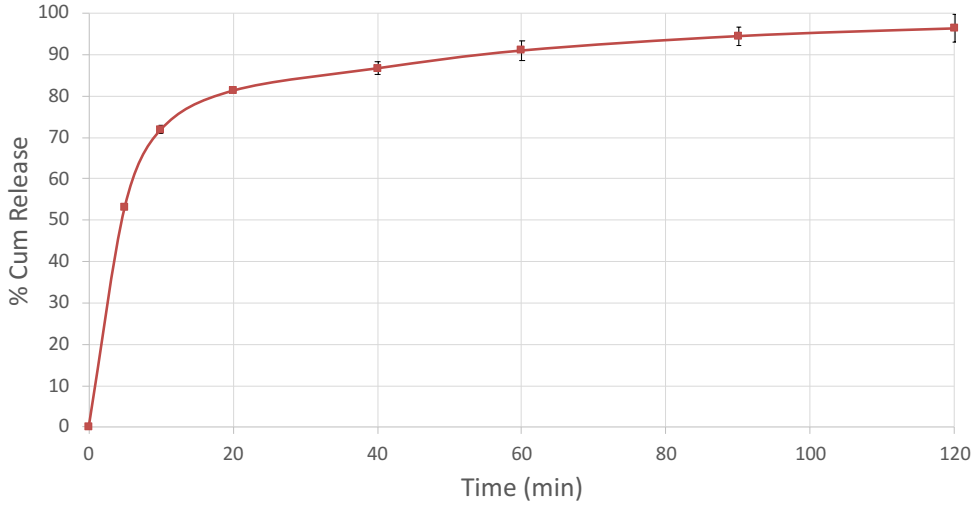

Figure 16. Cumulative release of L1 from $pSiO_2$ in HEPES buffer in the presence of Cu (II).

3.2 Py_2N_2 (L2) Loading and Release

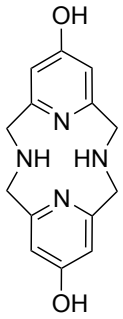

Figure 17. The structure of Py_2N_2 (L2)

Figure 17 shows L2 and **Figure 18** shows the calibration curves of L2 in DMSO, HEPES, and HEPES + Cu (II).

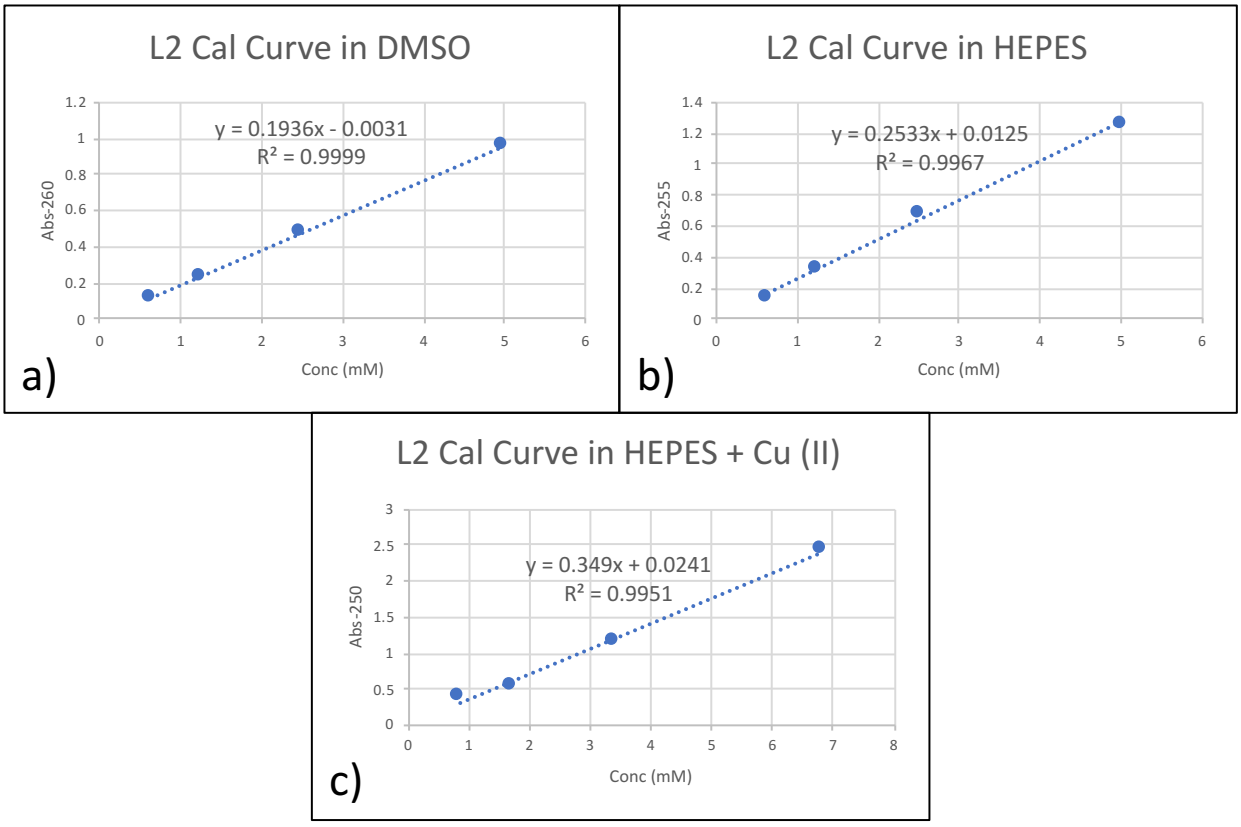

Figure 18. The L2 calibration curves in a) DMSO, b) HEPES, c) HEPES + Cu (II). Absorbance is measured on the y-axis and concentration in mM is measured on the x-axis. The absorbance coefficients obtained are a) 0.194, b) 0.253, c) 0.349.

Encapsulation efficiency for L2 was determined to be 10% as shown in **Figure 19**. This value was used to calculate the percent release in each of the release trials for L2.

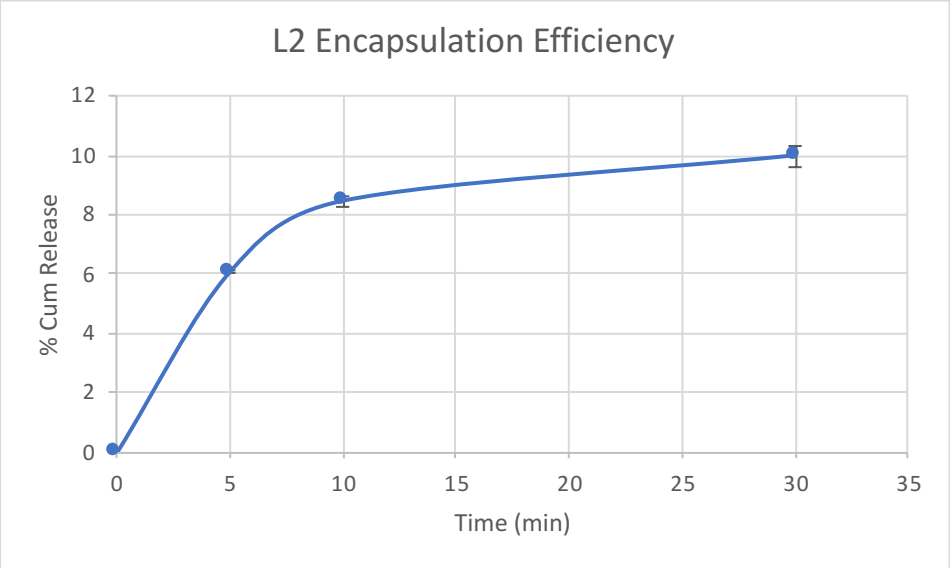

Figure 19. L2 encapsulation efficiency of 10% measured in DMSO.

The release profile of L2 from $pSiO_2$ in HEPES buffer is shown in **Figure 20** where a much slower rate of release is observed than what was observed with L1. While 45% of L1 is released within the first 5 minutes, only 15% of L2 is released within the same time period.

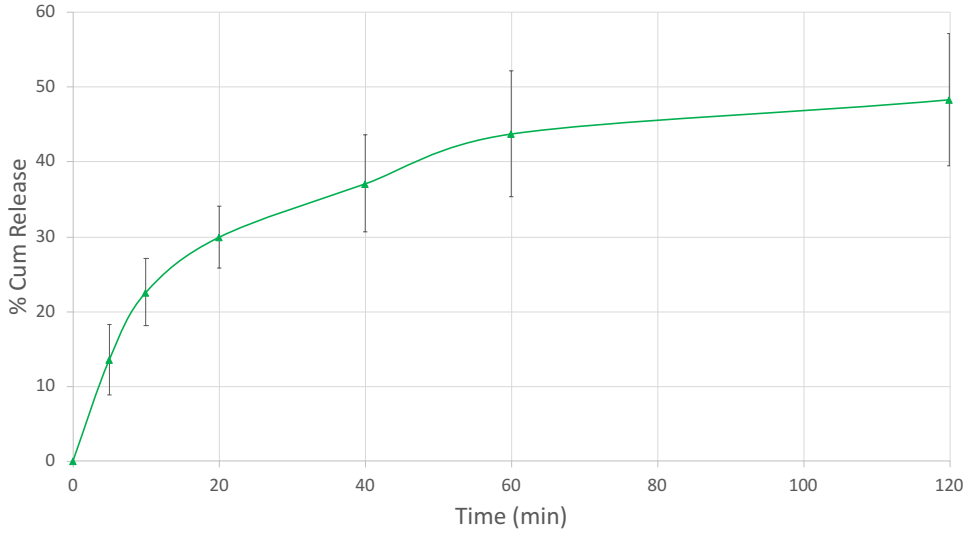

Figure 20. Cumulative release of L2 from $pSiO_2$ in HEPES buffer

When the release is done in the presence of Cu (II), as seen in **Figure 21**, L2 proves again to be slower than L1. However, it is important to note that there was some precipitation observed with the Cu once L2 was added at physiological pH. This could lead to results that are artificially lower than the true value. However, since the results in the absence of Cu yielded similar decrease in release rate without possible precipitation, it is safe to assume that the results are close to the true value.

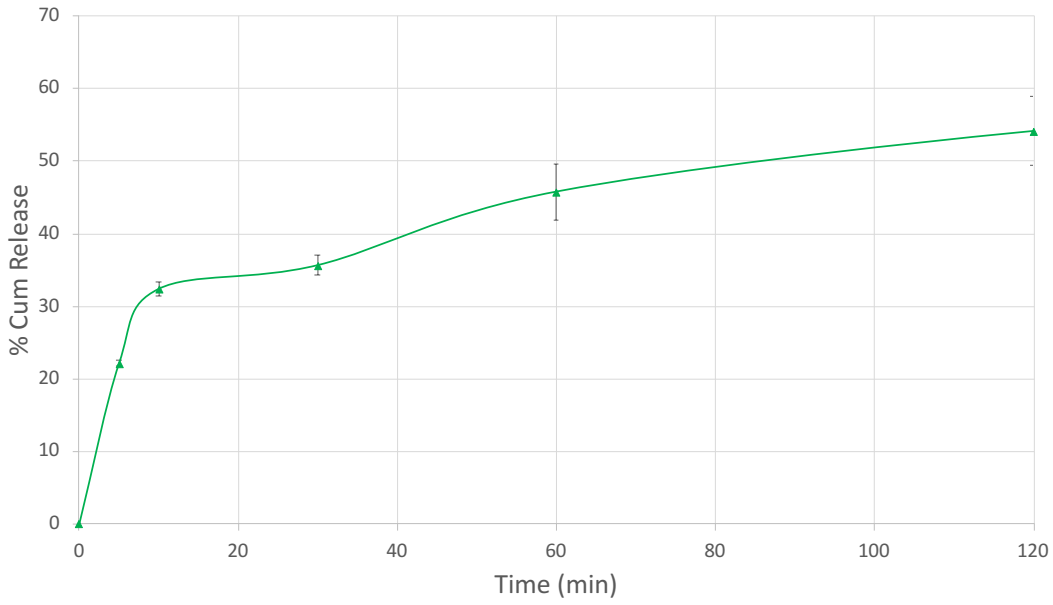

Figure 21. Cumulative release of L2 from $pSiO_2$ in HEPES buffer in the presence of Cu (II)

3.3 $^{Cl}Py_2N_2$ (L3) Loading and Release

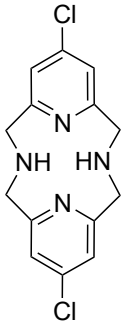

Figure 22. The structure of $^{Cl}Py_2N_2$ (L3)

Figure 22 shows L3 and **Figure 23** shows the calibration curves of L3 in DMSO, HEPES, and HEPES + Cu (II).

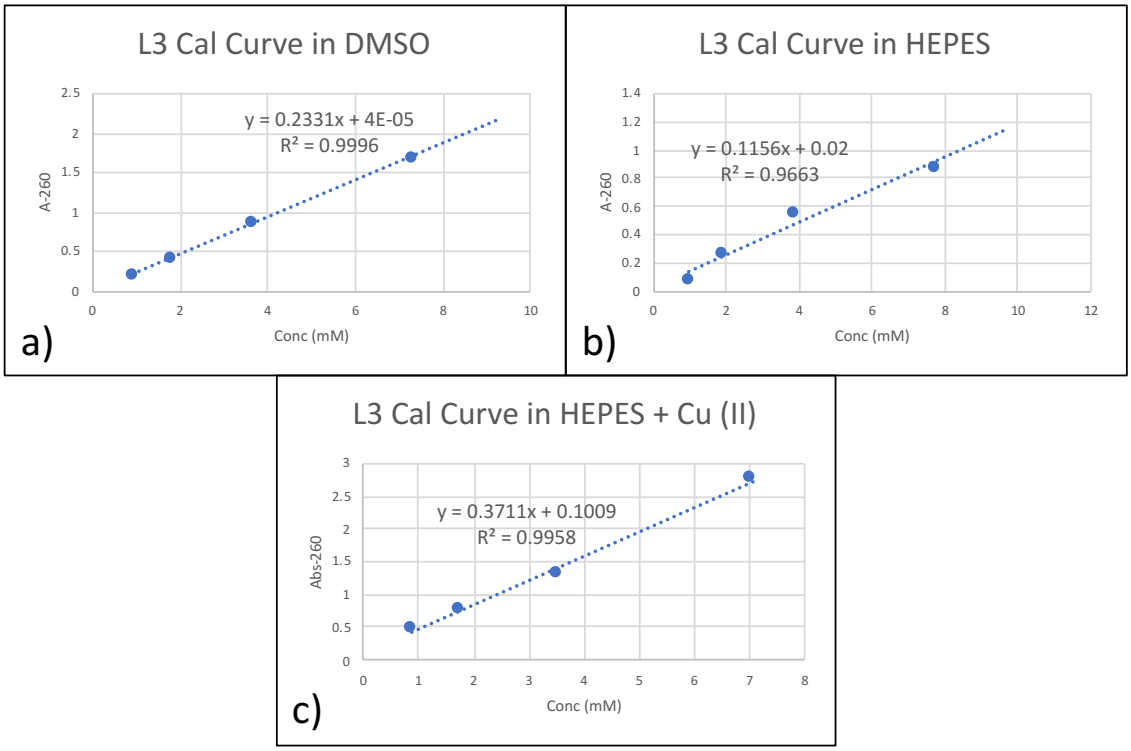

Figure 23. The L3 calibration curves in a) DMSO, b) HEPES, c) HEPES + Cu (II). The absorbance coefficients obtained are a) 0.233, b) 0.116, c) 0.371.

Encapsulation efficiency for L3 was determined to be 16% as shown in **Figure 24**. This value was used to calculate the percent release in each of the release trials for L3.

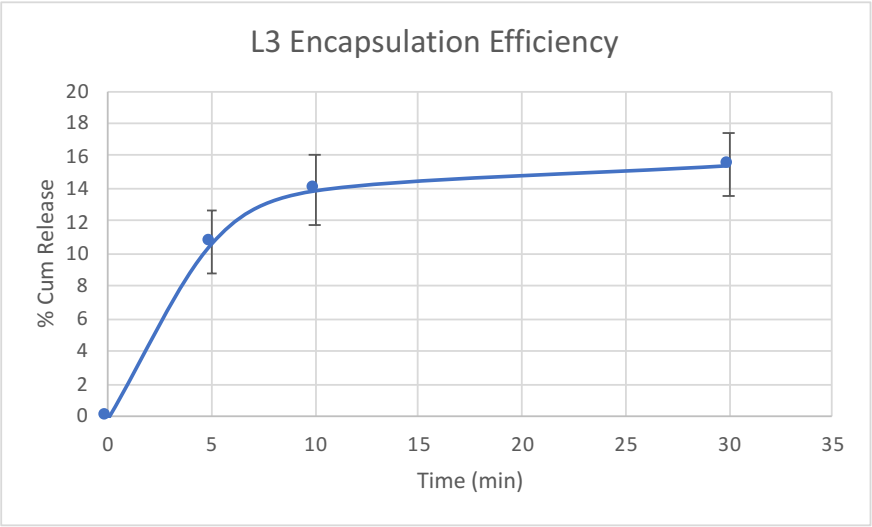

Figure 24. L3 encapsulation efficiency of 16% measured in DMSO.

The release profile of L3 is shown in **Figure 25** where the rate is still slower than that of L1 but is faster than the rate observed with L2. It is worth noting that the percent release in this graph is greater than 100%. This means that the encapsulation efficiency measured was not accurate for this series of measurements. This is an issue that was regularly encountered and is likely the result of solvent entrapment that takes place during loading. Some of the ethanol in which the chelating agents are dissolved gets entrapped in the pores of the silica as well making exact loading difficult to measure. However, of all the methods used during this work, encapsulation efficiency in DMSO does yield the most accurate results. Maximum loading, while could be very useful, is not the main focus of this study. The rate at which the profile reaches its plateau is what is of more interest here.

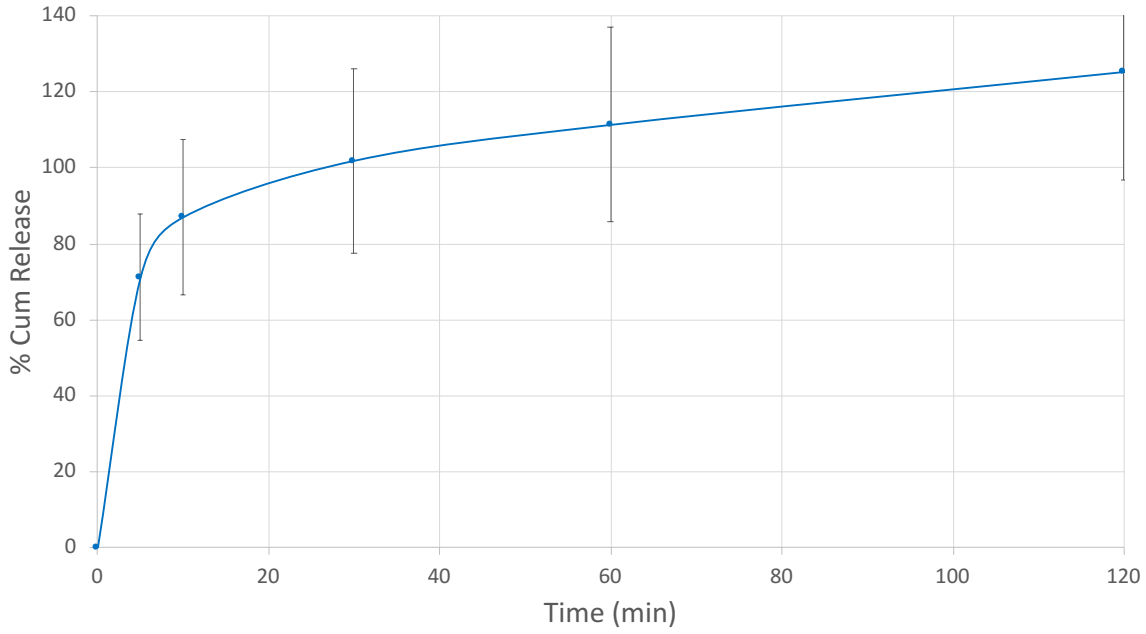

Figure 25. Cumulative release of L3 from $pSiO_2$ in HEPES buffer

When the release is done in the presence of Cu (II), as seen in **Figure 26**, L3 again shows a rate slower than that of L1 but faster than L2. The results are consistent with or without the presence of Cu (II) in the HEPES buffer.

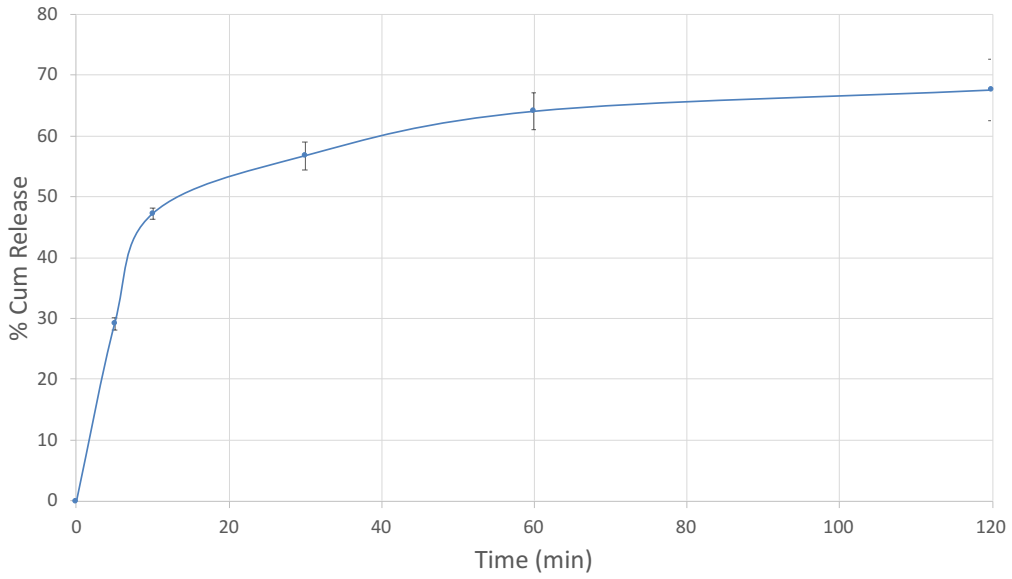

Figure 26. Cumulative release of L3 from $pSiO_2$ in HEPES buffer in the presence of Cu (II)

4 Conclusions and Future Work

When the release profiles of the three macrocycles are compared, several observations could be made. **Figure 27** shows the release profiles of the three molecules in HEPES without Cu.

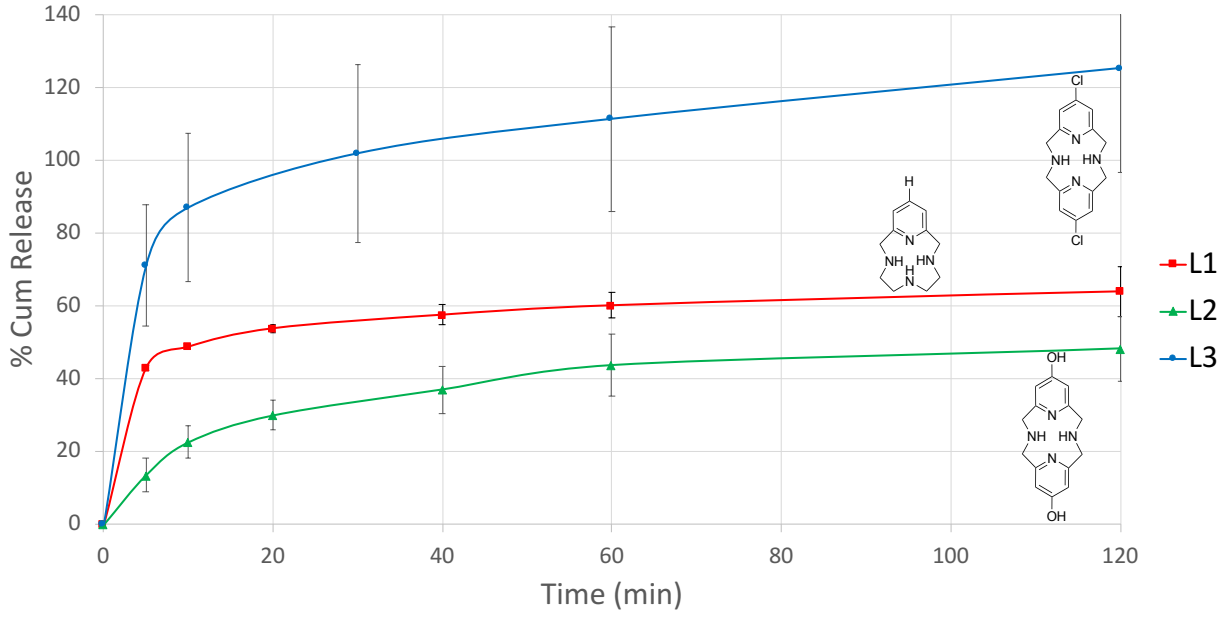

Figure 27. Cumulative release of L1, L2, & L3 from $pSiO_2$ in HEPES buffer.

The dimer macrocycles showed a slower release profile proving to be better candidates if slow release is targeted for a drug of interest. This indicates that the larger molecules are capable of being stuck in the $pSiO_2$ pores better than monomers slowing down their release and prolonging the overall drug release time. This is also seen in **Figure 28** where the three profiles are shown in the presence of Cu.

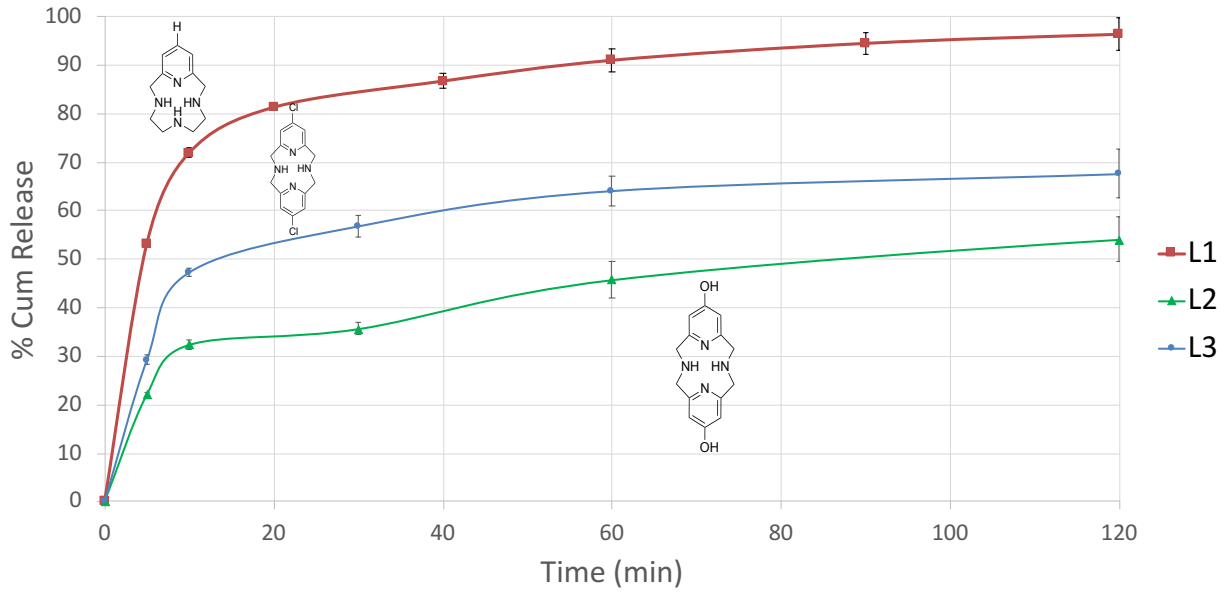

Figure 28. Cumulative release of L1, L2, & L3 from $pSiO_2$ in HEPES buffer in the presence of Cu (II)

Furthermore, it is clear that the L2 OH-substituted dimer showed the slowest rate of release overall. This likely points to the hydrogen bonding between the substituent group of the macrocycle and the oxygen atoms in the silica as another slowing interaction that keeps the macrocycle within the pores for longer time periods.

For the future, macrocycles with antioxidative capabilities to combat neurodegenerative diseases like Alzheimer's Disease could continue being structured in ways that can optimize their release in porous nanoscale drug delivery systems, such as the mesoporous SiO_2 system used in

this work. Larger molecules, such as trimers or tetramers, should be developed to find the optimal macrocycle size. Substituent groups capable of hydrogen bonding should also be added to future chelating agents to optimize the interaction between the drugs and the $pSiO_2$ carriers. These therapeutic candidates could then be tested with protein assay experiments in the presence of amyloid ß to measure their effectiveness in inhibiting or breaking apart Aß aggregates.

References

1. 2022 Alzheimer's Disease Facts and Figures. *Alzheimer's & Dementia* **2022**, *18* (4), 700–789. DOI: 10.1002/alz.12638

2. Mrdenovic, D.; Zarzycki, P.; Majewska, M.; Pieta, I. S.; Nowakowski, R.; Kutner, W.; Lipkowski, J.; Pieta, P. Inhibition of Amyloid β-Induced Lipid Membrane Permeation and Amyloid β Aggregation by K162. *ACS Chemical Neuroscience* **2021**, *12* (3), 531–541. DOI: 10.1021/acschemneuro.0c00754

3. Brothers, H. M.; Gosztyla, M. L.; Robinson, S. R. The Physiological Roles of Amyloid-β Peptide Hint at New Ways to Treat Alzheimer's Disease. *Frontiers in Aging Neuroscience* **2018**, *10,* 118. DOI: 10.3389/fnagi.2018.00118

4. Hellstrand, E.; Boland, B.; Walsh, D. M.; Linse, S. Amyloid β-Protein Aggregation Produces Highly Reproducible Kinetic Data and Occurs by a Two-Phase Process. *ACS Chemical Neuroscience* **2009**, *1* (1), 13–18. DOI: 10.1021/cn900015v

5. Silverman, J. M.; Gibbs, E.; Peng, X.; Martens, K. M.; Balducci, C.; Wang, J.; Yousefi, M.; Cowan, C. M.; Lamour, G.; Louadi, S.; Ban, Y.; Robert, J.; Stukas, S.; Forloni, G.; Hsiung, G.Y. R.; Plotkin, S. S.; Wellington, C. L.; Cashman, N. R. A Rational Structured Epitope Defines a Distinct Subclass of Toxic Amyloid-Beta Oligomers. *ACS Chemical Neuroscience* **2018**, *9* (7), 1591–1606. DOI: 10.1021/acschemneuro.7b00469

6. Maity, B. K.; Das, A. K.; Dey, S.; Moorthi, U. K.; Kaur, A.; Dey, A.; Surendran, D.; Pandit, R.; Kallianpur, M.; Chandra, B.; Chandrakesan, M.; Arumugam, S.; Maiti, S. Ordered and Disordered Segments of Amyloid-β Drive Sequential Steps of the Toxic Pathway. *ACS Chemical Neuroscience* **2019**, *10* (5), 2498–2509. DOI: 10.1021/acschemneuro.9b00015

7. Kamat, P. K.; Kalani, A.; Rai, S.; Swarnkar, S.; Tota, S.; Nath, C.; Tyagi, N. Mechanism of Oxidative Stress and Synapse Dysfunction in the Pathogenesis of Alzheimer's Disease: Understanding the Therapeutics Strategies. *Molecular Neurobiology* **2014**, *53* (1), 648–661. DOI: 10.1007/s12035-014-9053-6

8. Opazo, C. M.; Greenough, M. A.; Bush, A. I. Copper: From Neurotransmission to Neuroproteostasis. *Frontiers in Aging Neuroscience* **2014**, *6*, 143. DOI: 10.3389/fnagi.2014.00143

9. Gaier, E. D.; Eipper, B. A.; Mains, R. E. Copper Signaling in the Mammalian Nervous System: Synaptic Effects. *Journal of Neuroscience Research* **2012**, *91* (1), 2-19. DOI: 10.1002/jnr.23143

10. Ackerman, C. M.; Chang, C. J. Copper Signaling in the Brain and Beyond. *Journal of Biological Chemistry* **2018**, *293*(13), 4628–4635. DOI: 10.1074/jbc.R117.000176

11. Posadas, Y.; Parra-Ojeda, L.; Perez-Cruz, C.; Quintanar, L. Amyloid β Perturbs Cu(II) Binding to the Prion Protein in a Site-Specific Manner: Insights into Its Potential

Neurotoxic Mechanisms. *Inorganic Chemistry* **2021**, *60* (12), 8958–8972. DOI: 10.1021/acs.inorgchem.1c00846

12. Hung, Y. H.; Bush, A. I.; Cherny, R. A. Copper in the Brain and Alzheimer's Disease. *JBIC Journal of Biological Inorganic Chemistry* **2009**, *15* (1), 61–76. DOI: 10.1007/s00775-009-0600-y

13. Gupta, M.; Bogdanowicz, T.; Reed, M. A.; Barden, C. J.; Weaver, D. F. The Brain Exposure Efficiency (Bee) Score. *ACS Chemical Neuroscience* **2019**, *11* (2), 205–224. DOI: 10.1021/acschemneuro.9b00650h

14. Gupta, M.; Lee, H. J.; Barden, C. J.; Weaver, D. F. The Blood–Brain Barrier (BBB) Score. *Journal of Medicinal Chemistry* **2019**, *62* (21), 9824–9836. DOI: 10.1021/acs.jmedchem.9b01220

15. Tibbitt, M. W.; Dahlman, J. E.; Langer, R. Emerging Frontiers in Drug Delivery. *Journal of the American Chemical Society* **2016**, *138* (3), 704–717. DOI: 10.1021/jacs.5b09974

16. Brown, T. D.; Habibi, N.; Wu, D.; Lahann, J.; Mitragotri, S. Effect of Nanoparticle Composition, Size, Shape, and Stiffness on Penetration across the Blood–Brain Barrier. *ACS Biomaterials Science & Engineering* **2020**, *6* (9), 4916–4928. DOI: 10.1021/acsbiomaterials.0c00743

17. Farokhzad, O. C.; Langer, R. Impact of Nanotechnology on Drug Delivery. *ACS Nano* **2009**, *3* (1), 16–20. DOI: 10.1021/nn900002m

18. Gu, F.; Zhang, L.; Teply, B. A.; Mann, N.; Wang, A.; Radovic-Moreno, A. F.; Langer, R.; Farokhzad, O. C. Precise Engineering of Targeted Nanoparticles by Using Self-Assembled Biointegrated Block Copolymers. *Proceedings of the National Academy of Sciences* **2008**, *105* (7), 2586–2591. DOI: 10.1073/pnas.0711714105

19. Decuzzi, P.; Pasqualini, R.; Arap, W.; Ferrari, M. Intravascular Delivery of Particulate Systems: Does Geometry Really Matter? *Pharmaceutical Research* **2008**, *26* (1). DOI: 10.1007/s11095-008-9697-x

20. Moodley, K.; Pillay, V.; Choonara, Y. E.; du Toit, L. C.; Ndesendo, V. M.; Kumar, P.; Cooppan, S.; Bawa, P. Oral Drug Delivery Systems Comprising Altered Geometric Configurations for Controlled Drug Delivery. *International Journal of Molecular Sciences* **2011**, *13* (1), 18–43. DOI: 10.3390/ijms13010018

21. Santini, Jr., J. T.; Richards, A. C.; Scheidt, R.; Cima, M. J.; Langer, R. Microchips as Controlled Drug-Delivery Devices. *Angewandte Chemie International Edition* **2000**, *39* (14), 2396–2407. PMID: 10941095

22. McInnes, S. J.; Szili, E. J.; Al-Bataineh, S. A.; Vasani, R. B.; Xu, J.; Alf, M. E.; Gleason, K. K.; Short, R. D.; Voelcker, N. H. Fabrication and Characterization of a Porous Silicon Drug Delivery System with an Initiated Chemical Vapor Deposition Temperature-

Responsive Coating. *Langmuir* **2015**, *32* (1), 301–308. DOI: 10.1021/acs.langmuir.5b03794

23. Le, N. T.; Kalluri, J. R.; Loni, A.; Canham, L. T.; Coffer, J. L. Biogenic Nanostructured Porous Silicon as a Carrier for Stabilization and Delivery of Natural Therapeutic Species. *Molecular Pharmaceutics* **2017**, *14* (12), 4509–4514. DOI: 10.1021/acs.molpharmaceut.7b00638

24. Canham, L. Tunable Properties of Porous Silicon. In: Handbook of Porous Silicon. *Springer, Cham* **2018**, 283-290 DOI: 10.1007/978-3-319-71381-6_19

25. Canham, L. Porous Silicon Application Survey. In: Handbook of Porous Silicon. *Springer, Cham* **2018**, 1089-1097 DOI: 10.1007/978-3-319-71381-6_74

26. Kalluri, J. R.; West, J.; Akkaraju, G. R.; Canham, L. T.; Coffer, J. L. Plant-Derived Tandem Drug/Mesoporous Silicon Microcarrier Structures for Anti-Inflammatory Therapy. *ACS Omega* **2019**, *4* (5), 8359–8364. DOI: 10.1021/acsomega.9b00127

27. Johnston, H. M.; Pota, K.; Barnett, M. M.; Kinsinger, O.; Braden, P.; Schwartz, T. M.; Hoffer, E.; Sadagopan, N.; Nguyen, N.; Yu, Y.; Gonzalez, P.; Tircsó, G.; Wu, H.; Akkaraju, G.; Chumley, M. J.; Green, K. N. Enhancement of the Antioxidant Activity and Neurotherapeutic Features through Pyridol Addition to Tetraazamacrocyclic Molecules. *Inorganic Chemistry* **2019**, *58* (24), 16771–16784. DOI: 10.1021/acs.inorgchem.9b02932

28. Lincoln, K. M.; Offutt, M. E.; Hayden, T. D.; Saunders, R. E.; Green, K. N. Structural, Spectral, and Electrochemical Properties of Nickel(Ii), Copper(Ii), and Zinc(Ii) Complexes Containing 12-Membered Pyridine- and Pyridol-Based Tetra-Aza Macrocycles. *Inorganic Chemistry* **2014**, *53* (3), 1406–1416. DOI: 10.1021/ic402119s

29. Mekhail, M. A.; Pota, K.; Schwartz, T. M.; Green, K. N. Functionalized Pyridine in Pyclen-Based Iron(Iii) Complexes: Evaluation of Fundamental Properties. *RSC Advances* **2020**, *10* (52), 31165–31170. DOI: 10.1039/d0ra05756h

30. Wang, J.; Wang, K.; Zhu, Z.; He, Y.; Zhang, C.; Guo, Z.; Wang, X. Inhibition of Metal-Induced Amyloid β-Peptide Aggregation by a Blood–Brain Barrier Permeable Silica–Cyclen Nanochelator. *RSC Advances* **2019**, *9* (25), 14126–14131. DOI: 10.1039/c9ra02358e